Molecular Horticulture

RESEARCH ARTICLE

Open Access

Seizing the key nodes in glabridin biosynthesis network: identification of enzymes for producing licorice hairy roots with high levels of glabridin

Ningxin Jiang[1,2,3†], Xiaoling Ma[1,4†], Yangxu Wu[1,3], Xiaoyi Wei[1,2,3], Yuping Li[1], Xinyan Guo[1,3], Hongxia Wang[3,5], Wei Sun[6], Ling Yuan[7*], Ying Wang[1,2,3*] and Yongqing Li[1,2,3*]

Abstract

Glabridin holds significant value in the pharmaceutical and cosmetics industry. Due to the challenges associated with chemical synthesis, *Glycyrrhiza glabra* (licorice) remains the only source of glabridin. However, its naturally low content is insufficient to meet the increasing market demand. In this study, several inducers of glabridin accumulation—alkali stress, salt–alkali stress, hydroxylamine, 5-azacytidine, and methyl jasmonate (MeJA)—were identified. Using integrated multi-omics analyses and in vitro enzyme assays, two interconnected biosynthetic routes were elucidated: an OMT/ODMT-dependent pathway involving methylation-demethylation cycles and an OMT/ODMT-independent route. Five enzymes, GgIFR (isoflavone reductase), GgTHIS1/2 (7,2′,4′-trihydroxyisoflavanol synthases), GgPTS (pterocarpan synthase), GgPTR1/4 (pterocarpan reductases), and GgODMT (*O*-demethyltransferase), were functionally validated. Using an optimized *Agrobacterium rhizogenes*-mediated transformation system, we generated transgenic hairy root lines overexpressing these enzymes were generated. *GgIFR*-overexpressing lines achieved a 44-fold increase in glabridin content (0.507 mg/g DW), comparable to levels in 4-year-old wild roots. This study not only elucidates the complex biosynthetic network of glabridin biosynthesis but also establishes a scalable and sustainable hairy root platform for its industrial production via synthetic biology.

Keywords *Glycyrrhiza glabra*, Glabridin, Isoflavonoid biosynthesis, Hairy roots, Synthetic biology

†Ningxin Jiang and Xiaoling Ma contributed equally to this work.

*Correspondence:
Ling Yuan
lyuan3@uky.edu
Ying Wang
yingwang@scib.ac.cn
Yongqing Li
liyongqing@scbg.ac.cn
[1] State Key Laboratory of Plant Diversity and Specialty Crops, Guangdong Provincial Key Laboratory of Applied Botany, South China Botanical Garden, Chinese Academy of Sciences, Guangzhou 510650, China
[2] College of Life Science, Gannan Normal University, Ganzhou, Jiangxi 341000, P.R. China
[3] University of Chinese Academy of Sciences, Beijing 100049, China
[4] Department of Basic Medical Science, Quanzhou Medical College, Quanzhou, Fujian 362011, China
[5] Shanghai Key Laboratory of Plant Functional Genomics and Resources, Shanghai Chenshan Botanical Garden, Shanghai 201602, China
[6] Key Laboratory of Beijing for Identification and Safety Evaluation of Chinese Medicine, Institute of Chinese Materia Medica, China Academy of Chinese Medical Sciences, Beijing 100700, China
[7] Department of Plant and Soil Sciences, University of Kentucky, Lexington, KY 40506, USA

Core

This study identified inducers of glabridin accumulation and elucidated two interconnected biosynthetic pathways through multi-omics analyses and enzyme characterization. Functional validation of key enzymes and development of transgenic hairy root system led to a 44-fold increase in glabridin yield. The research offers a scalable platform for the sustainable industrial production of glabridin.

© The Author(s) 2026. **Open Access** This article is licensed under a Creative Commons Attribution 4.0 International License, which permits use, sharing, adaptation, distribution and reproduction in any medium or format, as long as you give appropriate credit to the original author(s) and the source, provide a link to the Creative Commons licence, and indicate if changes were made. The images or other third party material in this article are included in the article's Creative Commons licence, unless indicated otherwise in a credit line to the material. If material is not included in the article's Creative Commons licence and your intended use is not permitted by statutory regulation or exceeds the permitted use, you will need to obtain permission directly from the copyright holder. To view a copy of this licence, visit http://creativecommons.org/licenses/by/4.0/. The Creative Commons Public Domain Dedication waiver (http://creativecommons.org/publicdomain/zero/1.0/) applies to the data made available in this article, unless otherwise stated in a credit line to the data.

Gene & accession numbers

The accession numbers are: GgIFR (C_AA113735.1), GgODMT (C_AA113736.1), GgPTR1 (C_AA113737.1), GgPTR4(C_AA113738.1), GgPTS (C_AA113739.1), GgTHIS1 (C_AA113740.1), GgTHIS2 (C_AA113741.1).

Introduction

Glycyrrhiza glabra (licorice), a perennial herb in the Leguminosae family, has long been used in traditional medicine systems worldwide. It is rich in diverse bioactive compounds that contribute to its wide-ranging pharmacological properties (Wahab et al. 2021). Among these, glabridin is a particularly valuable compound with significant economic importance across multiple industries. In the cosmetics sector, its potent skin-whitening properties has earned it the nickname "whitening gold". However, glabridin is extremely scarce, only about 100 grams can be extracted from one ton of *G. glabra* roots, leading to high market prices and limiting its availability. In addition to its cosmetic applications, glabridin also exhibits strong anti-inflammatory and antioxidant activities, presenting opportunities for development in the food and pharmaceutical industries. These unique bioactivities, combined with limited natural supply, underscore glabridin's substantial economic significance.

Driven by growing demand, recent studies have focused on elucidating the complex biosynthetic pathway of glabridin in *Glycyrrhiza* species. Multi-omics approaches have facilitated the identification of key enzymes and regulatory networks involved in isoflavonoid biosynthesis (Li et al. 2024, 2025; Lu et al. 2025). Key enzymes such as isoflavone 4′-*O*-methyltransferase (I4′-OMT), isoflavone 2'-hydroxylase (I2'H), isoflavone reductase (IFR), vestitone reductase (VR), and pterocarpan synthase (PTS) have been individually characterized, particularly in the context of medicarpin biosynthesis, helping to clarify their roles in catalyzing key intermediate steps (Uchida et al. 2017; Lu et al. 2023). These findings laid the groundwork for pathway reconstruction in heterologous systems such as yeast, enabling *de novo* production of glabridin and related intermediates.

While *Saccharomyces cerevisiae* has been demonstrated to be useful for pathway engineering (Lu et al. 2023), *Agrobacterium rhizogenes*-mediated hairy roots have emerged as a promising platform for producing plant-derived natural products (Gerszberg and Wiktorek-Smagur 2022). Hairy roots offer unique advantages over traditional plant and cell cultures, including rapid growth, genetic and biochemical stability, and the ability to produce specialized metabolites without hormonal supplements (Srivastava and Srivastava. 2007). Their ability to grow in hormone-free media and adapt to bioreactor cultivation circumvents seasonal and environmental constraints. Furthermore, hairy roots are amenable to metabolic engineering tools such as CRISPR/Cas9 and transgenic overexpression, while promoter engineering can fine-tune tissue-specific expression to enhance pathway efficiency (Mirmazloum et al. 2024). For instance, in *Astragalus membranaceus* hairy roots, overexpression of the saponins pathway enzyme, *AmUGT15,* has successfully boosted production of the anticancer compound astragaloside by redirecting metabolic flux (Hwang et al. 2024). Similarly, CRISPR/Cas9-mediated knockout of competing pathway genes in licorice hairy roots has been shown to significantly enhance glycyrrhizin production, underscoring the potential of metabolic redirection in hairy root systems (Chiyo et al. 2024). Hairy roots also retain root-specific metabolic traits, making them especially effective for producing alkaloids, flavonoids, phenolics, and other specialized metabolites without external elicitation which has been demonstrated in over 100 medicinal plants (Morey and Peebles 2022; Wawrosch and Zotchev 2021). Collectively, these features make hairy roots an ideal system for both pathway elucidation and scalable production of valuable natural products.

In this study, we identified MeJA (methyl jasmonate), alkali stress, salt-alkali stress, hydroxylamine and 5-azacytidine (5-azaC) as inducers that significantly increase glabridin accumulation in *G. glabra* roots. Transcriptome analysis revealed candidate biosynthetic enzymes including IFR, 7,2',4'-Trihydroxyisoflavanol synthase (THIS), PTS, pterocarpan reductase (PTR), and *O*-demethyltransferase (ODMT), which were subsequently validated through in vitro assays. We also identified a prenyltransferase (PT) from *Cullen corylifolium* capable of catalyzing the prenylation of demethylmedicarpin, an essential step in glabridin biosynthesis. Additionally, we optimized the hairy root transformation system for *G. glabra* and generated transgenic lines overexpressing the validated enzymes. The hairy root lines overexpressing *GgIFR*, *GgTHIS1*, *GgPTS*, *GgPTR1,* and *GgODMT* showed significant accumulation of glabridin. This study not only confirms in vivo functionality of key enzymes in the glabridin pathway but also establishes a viable platform for future synthetic biology-based industrial production of glabridin.

Results

Spatial accumulation of glabridin in *G. glabra*

To investigate the tissue-specific accumulation of glabridin, its content was measured in various tissues of 4-year-old *G. glabra* plants (Fig. 1A). Glabridin was predominantly detected in the main and lateral roots, with concentrations ranging from 0.28 to 0.33 mg/g dry weight (DW). In contrast, glabridin was undetectable in aerial tissues such as leaves, stems, and lateral branches (Fig. 1B), consistent with previous reports indicating its localization primarily in the cork layer and necrotic regions of mature roots (Hayashi et al. 1996)

Given that licorice is naturally adapted to arid and semi-arid environment characterized by intense untraviolet radiation and saline-alkali soils, we explored whether environmental stressors could influence glabridin accumulation. Thirteen treatments were applied to 7-day-old *G. glabra* seedlings (Table S1), including abiotic stressors (drought, saline-alkali, salt, alkali, high temperature, oxidative stress, sucrose and UV-B irradiation), phytohormones (methyl jasmonate [MeJA] and abscisic acid [ABA]), and chemical modulators known to influence flavonoid biosynthesis (DNA methyltransferase inhibitor 5-azacytidine [5-azaC], histone acetyltransferase inhibitors, and hydroxylamine) (Ma et al. 2024; Zeng et al. 2025). Following treatment, root tissues were harvested and analyzed for glabridin content using HPLC. Notably, alkali stress, saline-alkali stress,

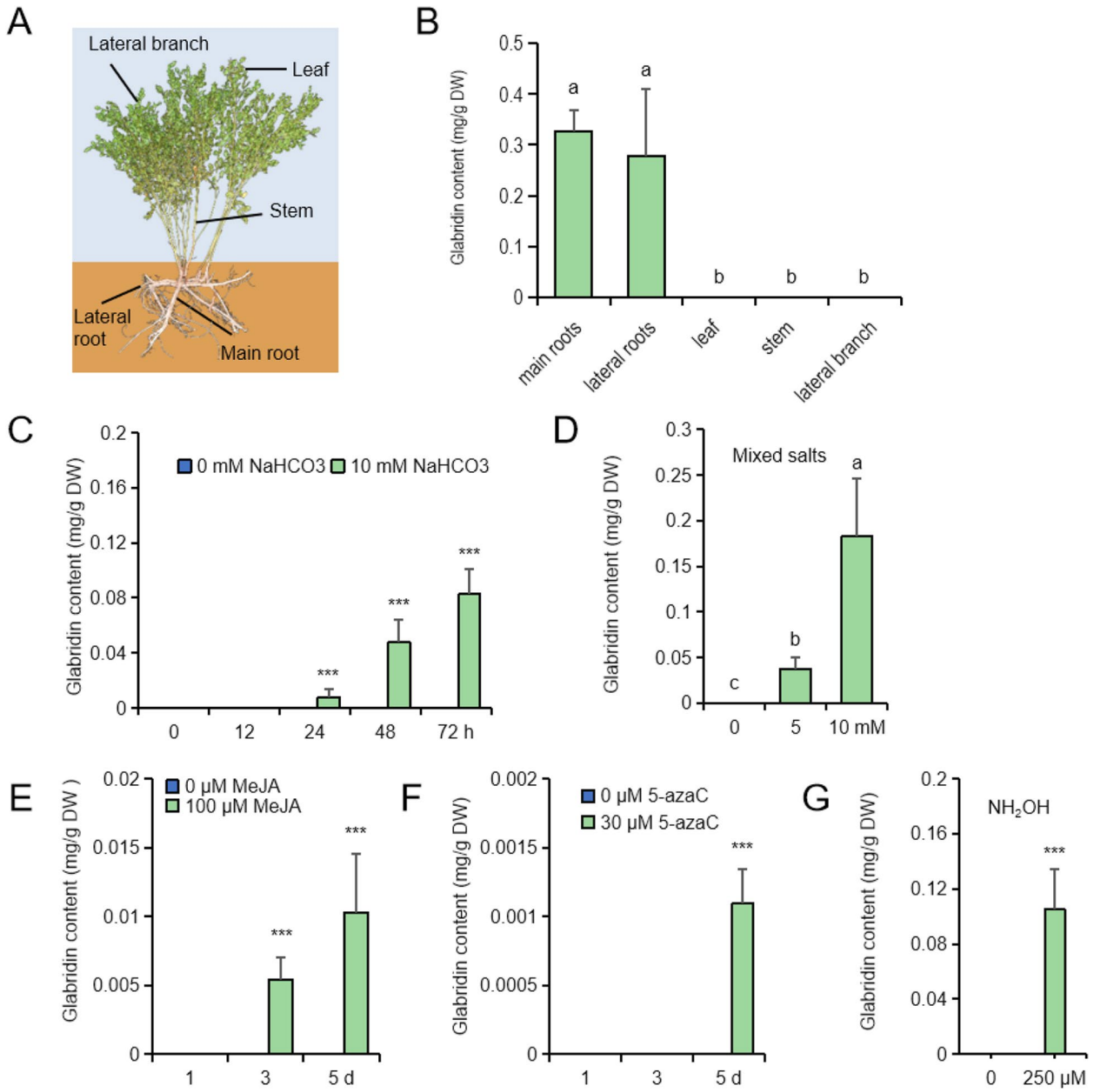


Fig. 1 The accumulation pattern of glabridin. Different tissues of 4-year-old *G. glabra* tested for glabridin (**A**), and the glabridin content in the different tissues (**B**). Glabridin content in the roots of 7-day-old seedlings of *G. glabra* treated with/without 10 mM $NaHCO_3$ (**C**), 5 mM and 10 mM mix salts (**D**), 100 μM MeJA (**E**), 30 μM 5-azaC (**F**), and 250 μM NH_2OH (**G**). Glabridin content were calculated based on dry weight. Data are presented as mean ± SD

hydroxylamine, 5-azaC, and MeJA significantly enhanced glabridin accumulation compared to controls (Fig. 1C–G). Among these, alkali stress, saline-alkali stress, and hydroxylamine exerted the most pronounced effects, achieving glabridin levels comparable to those found in 4-year-old roots after 72 h of treatment. MeJA produced moderate inductive effect, while 5-azaC had relatively weaker effect. To investigate the molecular mechanisms underlying glabridin biosynthesis, transcriptomic profiling (RNA-seq) was conducted on roots treated with alkali stress (the strongest inducer) and MeJA (broad-spectrum flavonoid activator) treatments (Fig. S1).

Identification and in vitro verification of enzymes involved in glabridin biosynthesis

Based on literature and our metabolomic datasets (Li et al. 2024, 2025), we proposed two interconnected glabridin biosynthetic pathways (Fig. 2). The *O*-methyltransferase/*O*-demethyltransferase (OMT/ODMT)-dependent pathway involves a methylation-demethylation cycle: daidzein is first methylated at *C*-4' by I4'-OMT to form medicarpin, followed by PTR-mediated reduction, PT-catalyzed prenylation, cyclase (CS)-driven cyclization, and ODMT-mediated demethylation. This pathway provides modularity and regulatory flexibility but introduces redundancy due to methyl-group cycling. In contrast, the OMT/ODMT-independent route bypasses methylation, using demethylmedicarpin as the precursor and relying on a streamlined cascade of reductases (IFR, VR/THIS, PTS, PTR), PT, and CS. This pathway is metabolically more efficient, eliminating energetically costly methylation-demethylation steps.

There are two ways to search for candidate genes involved in this pathway: homologous search and/or co-expression analysis. Genes with high sequence homology may have similar functions. For those steps with reported enzymes, homologous search may be more efficient to identify the best candidates. As for those novel steps, co-expression analysis is usually used since genes that co-express with glabridin may be involved in its biosynthesis. There are two parts in the biosynthetic pathway of glabridin: first, synthesis of medicarpin (**15**) or demethylmedicarpin (**13**); second, modification of **15** or **13**. Since the first part has been reported, homologous search was used to identify the best candidate genes. Co-expression analysis was used to identify candidate genes in the following steps.

Prior studies in soybean have demonstrated that IFR catalyzes the conversion of 2'-hydroxydaidzein (**10**) to 7,2',4'-trihydroxyisoflavanone (**11**) (Uchida et al. 2017). A BLAST search against the *G. glabra* genome using the *GmIFR* sequence identified a candidate gene, *Gg050003876*, with 80.56% sequence identity (Fig. S2A). This gene was significantly upregulated under MeJA or $NaHCO_3$ treatment (Fig. S2B). Next, the gene was heterologously expressed in *E. coli*, and the recombinant protein was subsequently assayed for enzymatic activity using **10** as substrate and nicotinamide adenine dinucleotide phosphate hydrogen (NADPH) as cofactor. High performance liquid chromatography (HPLC) analysis revealed a distinct peak at a retention time (RT) of 17.3 min, which is absent in control (RT = 19.1 min; Fig. 3A), while LC/MS analysisconfirmed the product identity - (*m/z* $[M+H]^+$ of 273.07; fragmented into *m/z* 135.04, *m/z* 163.04, *m/z* 245.08 and *m/z* 255.06; Fig. S2C-D), consistent with compound **11**. Therefore, *Gg050003876* encodes a functional IFR, and thus is designated as GgIFR.

It has been reported that VR from *M. sativa* catalyzes the reduction of vestitone (**9**) to form 7,2'-dihydroxy-4'-methoxyisoflavanol (**14**) (Guo and Paiva 1995). Recent studies in soybean have identified six reductases converting **11** to 7,2',4'-trihydroxyisoflavanol (**12**), with the most catalytically efficient isoforms designated as GmTHIS1 and GmTHIS2 (Sun et al. 2025). To identify orthologous enzymes in *G. glabra*, we characterized the VR/THIS gene family to identify reductases converting compound **11** to 7,2′,4′-trihydroxyisoflavanol (**12**). Of twenty-two candidates (Fig. S3A), three genes (*Gg010020471*, *Gg010020626*, and *Gg080009423*) clustered with *GmTHIS1*, *GmTHIS2*, and *MsVR*; however, *Gg080009423* could not be cloned from cDNA. Heterologous expression of *Gg010020471* and *Gg010020626* in *E. coli* and subsequent enzymatic assays using **11** and NADPH demonstrated that Gg010020626 catalyzed the conversion **11** to **12** with 12.55% efficiency, while Gg010020471 was inactive. Among 9 additional candidates (*Gg030032011*, *Gg040013722*, *Gg040013741*, *Gg040013732*, *Gg040014691*, *Gg040016889*, *Gg040017012*, *Gg050004518* and *Gg050005833*), only Gg040013732 exhibited weak activity (4.59%) (12.55%) (Fig. 3B, Fig. S4A-D). Gg010020626 and Gg040013732 were thus designated as GgTHIS1 and GgTHIS2, respectively. To evaluate vestitone (**9**) reduction to **14**, five enzymes (GgTHIS1, GgTHIS2, Gg010020471, Gg040016889, and Gg040017012) were tested. The activity ranking was: Gg010020471 > GgTHIS1 > Gg040016889 > Gg040017012 > GgTHIS2 (Fig. S4E-H). Sequence alignment revealed that GgTHIS1 shares >70% identity with GmTHIS1/GmTHIS2 and MsVR proteins, while GgTHIS2 shares ~30%, suggesting subfunctionalization, possibly reflecting distinct roles in stress-responsive ($NaHCO_3$-induced) and constitutive pathways (Table S3).

For the conversion of compound **12** to **13**, a BLAST search using the *G. echinata GePTS* (Uchida et al. 2017)

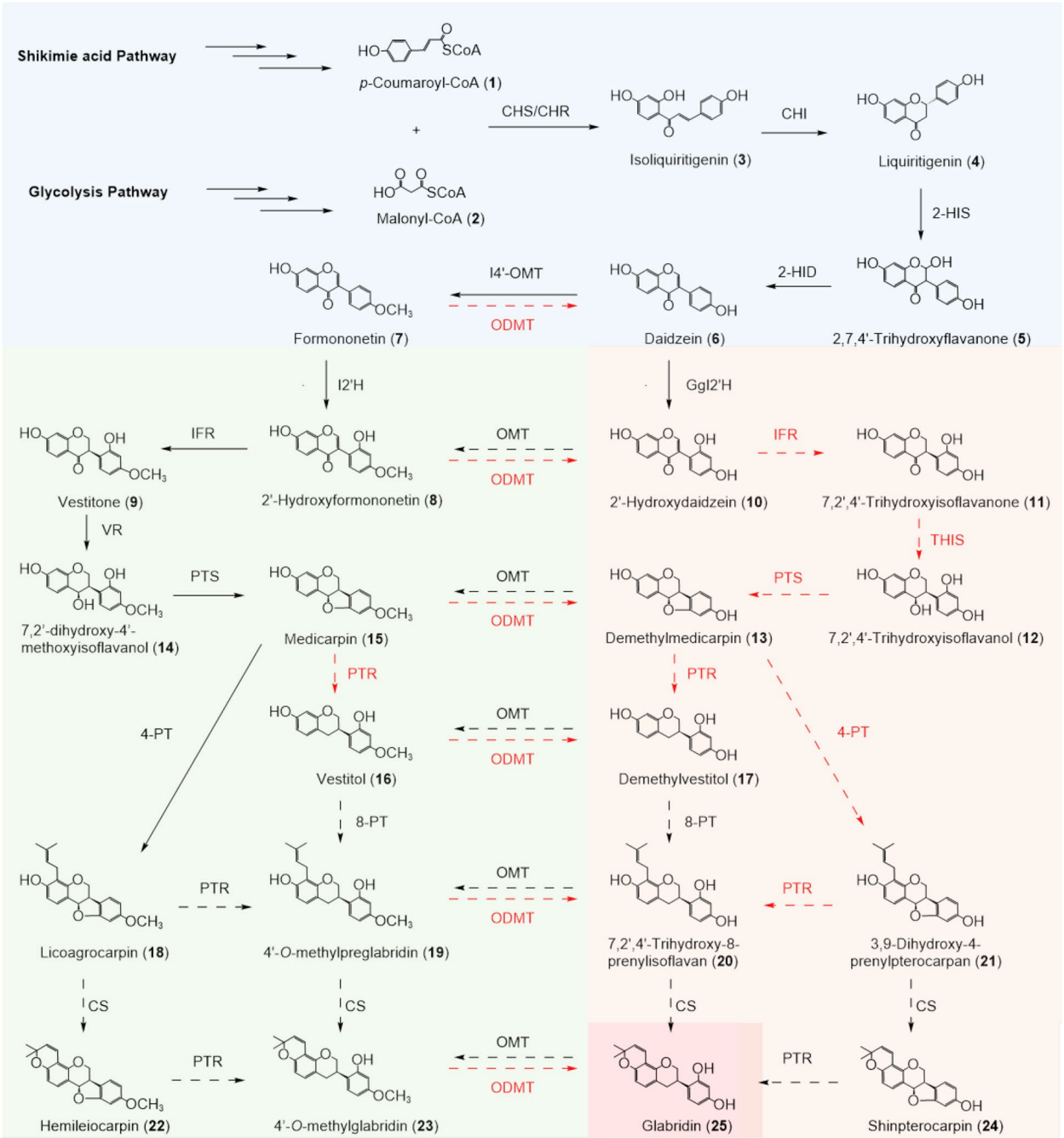


Fig. 2 Proposed glabridin biosynthetic pathway. CHS, chalcone synthase; CHI, chalcone isomerase; 2-HIS, 2-hydroxyisoflavanone synthase; 2-HID, 2-hydroxyisoflavanone dehydratase; I4'OMT, isoflavone 4'-*O*-methyltransferase; I2'H, isoflavone 2'-hydroxylase; IFR, isoflavone reductase; VR, vestitone reductase; THIS, 7,2',4'-trihydroxyisoflavanol synthase; PTS, pterocarpan synthase; PTR, pterocarpan reductase; PT, prenyltransferase; CS, cyclase; ODMT, *O*-demethyltransferase. Solid arrows represent characterized steps, dashed arrows represent uncharacterized steps in *G. glabra*, and red arrows represent steps identified in this study

identified a 576-bp *G. glabra* gene (95.83% identity; Fig. S5A) located on chromosome 7 (positions 28,406,063–28,406,638). The recombinant protein expressed in *E. coli* successfully catalyzed **13** formation from a crude **12**-enriched extract. HPLC revealed a peak at RT 14.1 min matching synthetic **13**, and LC-MS confirmed the identity (*m/z* $[M+H]^+$ 257.08; fragments: *m/z* 123.04, *m/z* 147.04; Fig. S5B–C). The enzyme was named GgPTS (Fig. 3C).

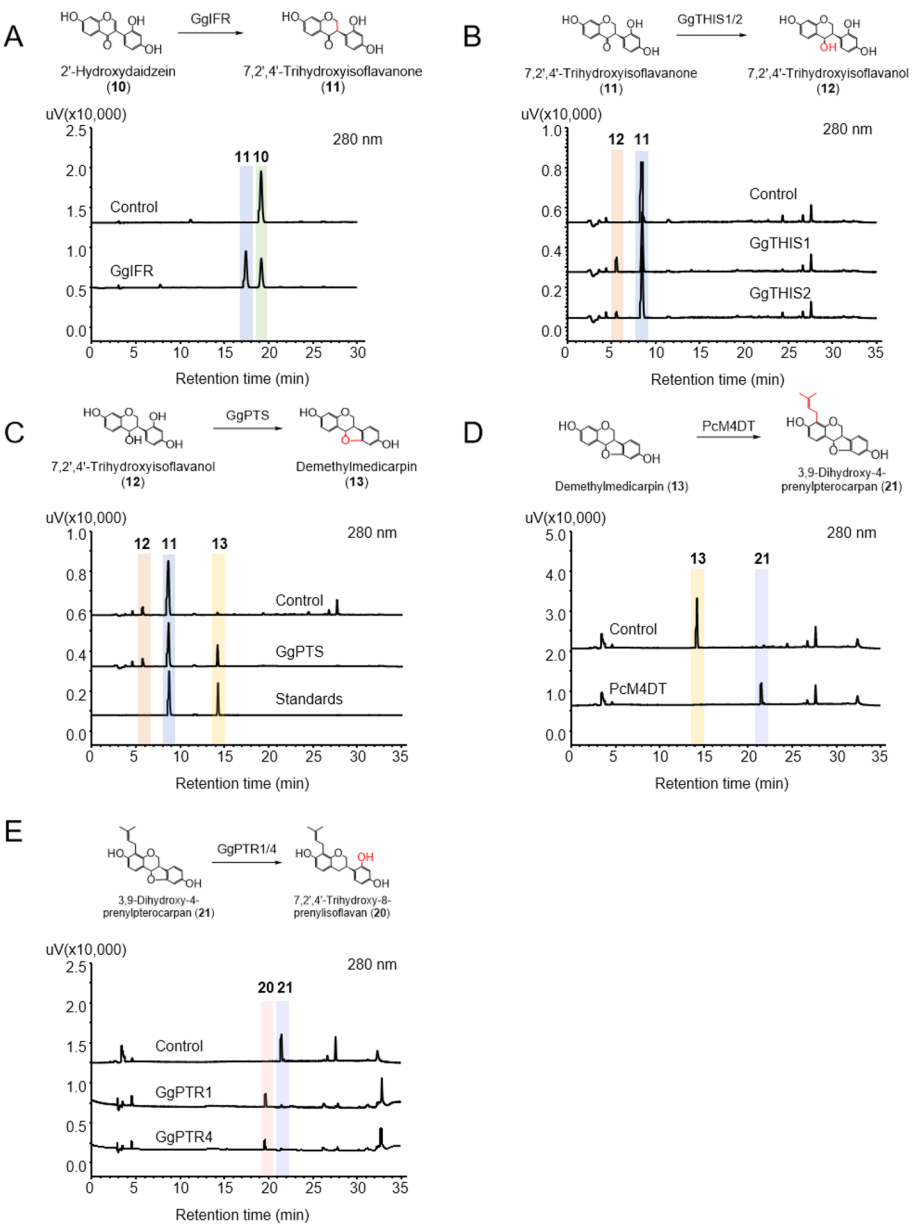


Fig. 3 Identification of the enzymes invovled in the glabridin bioynthesis excluding OMT and ODMT. Functional characterization of GgIFR (**A**), GgTHIS1/2 (**B**), GgPTS (**C**), PcM4DT (**D**) and GgPTR1/4 (**E**) are shown with the HPLC chromatograms of the enzymatic reactions

To identify enzymes responsible for the downstream steps (**13** → **25**), we screened PTR, PT, and CS by genome-wide screening of gene families coupled with transcriptome-based candidate prioritization. Twelve PTR genes were annotated, and seven of which (*Gg030033899*, *Gg030033561*, *Gg040015770*, *Gg040015832*, *Gg050003878*, *Gg050003876*, *Gg05 0004141*) were MeJA- and $NaHCO_3$-inducible (Fig. S6A-B). Five candidates (*Gg030033899*, *Gg030033561*, *Gg040015770*, *Gg040015832*, *Gg050003878*) were successfully cloned from cDNA. Of eight annotated PT genes, no one was induced by MeJA and $NaHCO_3$ treatments (Fig. S6C-D). For CS, recent studies have identified cytochrome P450 subfamily CYP71 members as glyceollin cyclases in soybean (Sun et al. 2025; Khatri et al. 2025; Xie et al. 2025). In our work, eleven CYP71 subfamily genes were identified. Six were induced by MeJA or $NaHCO_3$ treatment (*Gg030032002*, *Gg080008356*, *Gg050006811*, *Gg030032004*, *Gg030031443*, *Gg080008862*) and five were cloned except for *Gg050006811*.

Three potential enzymatic sequences were systematically evaluated. We first investigated the PT→PTR→CS pathway. For PTs, seven of eight were successfully cloned and tested in vitro with substrate **13**, yet no new product peaks were detected (Fig. S7A-B). We then examined PTs from other species and identified PcM4DT from *C. corylifolium*—reported to prenylate pterocarpan **15** at *C*-4 to yield **18** (He et al 2018). This catalytic specificity prompted us to test PcM4DT with structurally similar **13**. Remarkably, PcM4DT catalyzed **13** to produce a new peak (Fig. 3D). LC/MS analysis identified this product (*m/z* $[M+H]^+$: 325.14; fragments: *m/z* 123.04, *m/z* 147.04, *m/z* 191.11, *m/z* 269.08) (Fig. S7C), and NMR spectroscopy confirmed *C*-4 prenylation, identifying the product as **21** (Fig. S8). Subsequent GgPTRs assays with **21** revealed that both Gg040015770 and Gg030033561 converted **21** to **20** with >80% efficiency (Fig. S7D-G). However, microsomes expressing candidate GgCSs or soybean GmCSs (Glyma.11G062500 and Glyma.11G062600) failed to convert synthetic **20** to **25** using NADPH as cofactor (Fig. S9G-H). Next, we evaluated the PTR→PT→CS pathway. GgPTR candidates assayed with **13** revealed that Gg040015770 and Gg030033561 converted **13** to **17**, with conversion rates of 74.63% and 58.79%, respectively (Fig. S9A-D). Gg040015832 and Gg030033899 showed low expression in *E. coli*; their co-infiltration with **13** in tobacco also yielded no products (Fig. S11A-B). Seven GgPTs expressed in yeast microsomes failed to catalyze **17** with Dimethylallyl diphosphate (DMAPP) and Mg^{2+} (Fig. S9E-F). PcM4DT similarly showed no activity toward **17**. Critically, this pathway still required functional CS to convert **20** to **25**—a step that remained unresolved (Fig. S9G-H). Finally, the PT→CS→PTR pathway was excluded as CS candidates showed no activity toward **21** to **24**, and no PTR (including Gg040015770 or Gg030033561) catalyzed **24** to **25** (Fig. S10). Based on phylogenetic clustering with LjPTRs, Gg040015770 (LjPTR1 clade) and Gg030033561 (LjPTR4 clade) were designated as GgPTR1 and GgPTR4, respectively. These results delineate persistent functional constraints in late-stage pterocarpan modification toward **25** in *G. glabra*. Further characterization revealed that GgPTR1 and GgPTR4 catalyzed **15** to **16** reduction. In planta assays additionally demonstrated that Gg040015832 (*N. benthamiana* co-infiltration with **15**) produced a chromatographic peak consistent with **16**, indicating functional redundancy in pterocarpan reduction.

Functional characterization of demethylation enzymes in glabridin biosynthesis

Metabolomic profiling of *G. glabra* has identified the presence of methylated intermediates, including **15**, licoagrocarpin (**18**), and 4'-*O*-methylglabridin (**23**), suggesting the potential involvement of *O*-demethylases in glabridin biosynthesis (Li et al. 2024, 2025). Given the established function of 2-oxoglutarate-dependent dioxygenases (2-ODDs) in catalyzing *O*-demethylation in specialized metabolism, as reported in *Papaver somniferum* and *Ocimum basilicum* (Hagel and Facchini 2010; Berim et al. 2015), we conducted a genome-wide search for 2-ODD family members in *G. glabra*, and identified 147 *Gg2-ODD* candidate genes. Through phylogenetic clustering with functionally characterized demethylases (ObF7ODM1 and PsT6ODM), we identified 14 Gg2-ODDs residing within the same evolutionary clade (Fig. S12A). Transcriptome analysis under MeJA and $NaHCO_3$ treatments revealed five 2-ODD genes with expression patterns correlating with glabridin accumulation: *Gg020027239* (upregulated by MeJA), *Gg040016436*, *Gg040016899*, and *Gg050004870* (co-induced by MeJA and $NaHCO_3$), and *Gg040016437* (induced by $NaHCO_3$) (Fig. S12B). These five candidates were prioritized for functional characterization.

Subcellular localization predictions via Cell-PLoc (http://www.csbio.sjtu.edu.cn/bioinf/Cell-PLoc-2/) suggested that all five Gg2-ODD proteins are cytoplasmic. Based on these predictions, each candidate was heterologously expressed in *E. coli* and subjected to in vitro enzymatic assays in the presence of α-ketoglutarate and Fe^{2+}. Among the tested enzymes, Gg040016436 catalyzed the *O*-demethylation of six structurally diverse substrates: formononetin (**7**), vestitone (**9**), **15**, vestitol (**16**), 4'-*O*-methylpreglabridin (**19**), and **23**. HPLC and LC-MS analyses confirmed the conversion of 4'-OCH_3 to 4'-OH in each case (Fig. 4, Fig. S12C-H), indicating broad substrate specificity. Based on these results, Gg040016436 was designated as GgODMT. Due to the lack of authentic standards, the catalytic activity of GgODMT toward additional potential intermediates: 2'-hydroxyformononetin (**8**), 7,2'-dihydroxy-4'-methoxyisoflavanol (**14**), **18**, and hemileiocarpin (**22**), could not be conclusively assessed. Optimization of enzymatic conditions using **23** as a substrate revealed that GgODMT functions most effectively at pH 6.0, 20 °C, with a 90 min incubation (Fig. S13). Kinetic analyses showed the highest substrate affinity for **23** (*Km* = 75.358 μM) that was followed by **19** > **7** > **9** > **16** > **15** (Table S2). These findings established GgODMT as a promiscuous *O*-demethyltransferase capable of catalyzing multiple demethylation steps within the glabridin biosynthetic network.

Optimization of *G. glabra* hairy root induction

To functionally validate glabridin biosynthetic genes in vivo, a reliable *Agrobacterium rhizogenes*-mediated hairy root system was established in *G. glabra*. Although previous studies have reported successful transformation in *G. glabra* (Tenea et al. 2008; Srivastava et al. 2019;

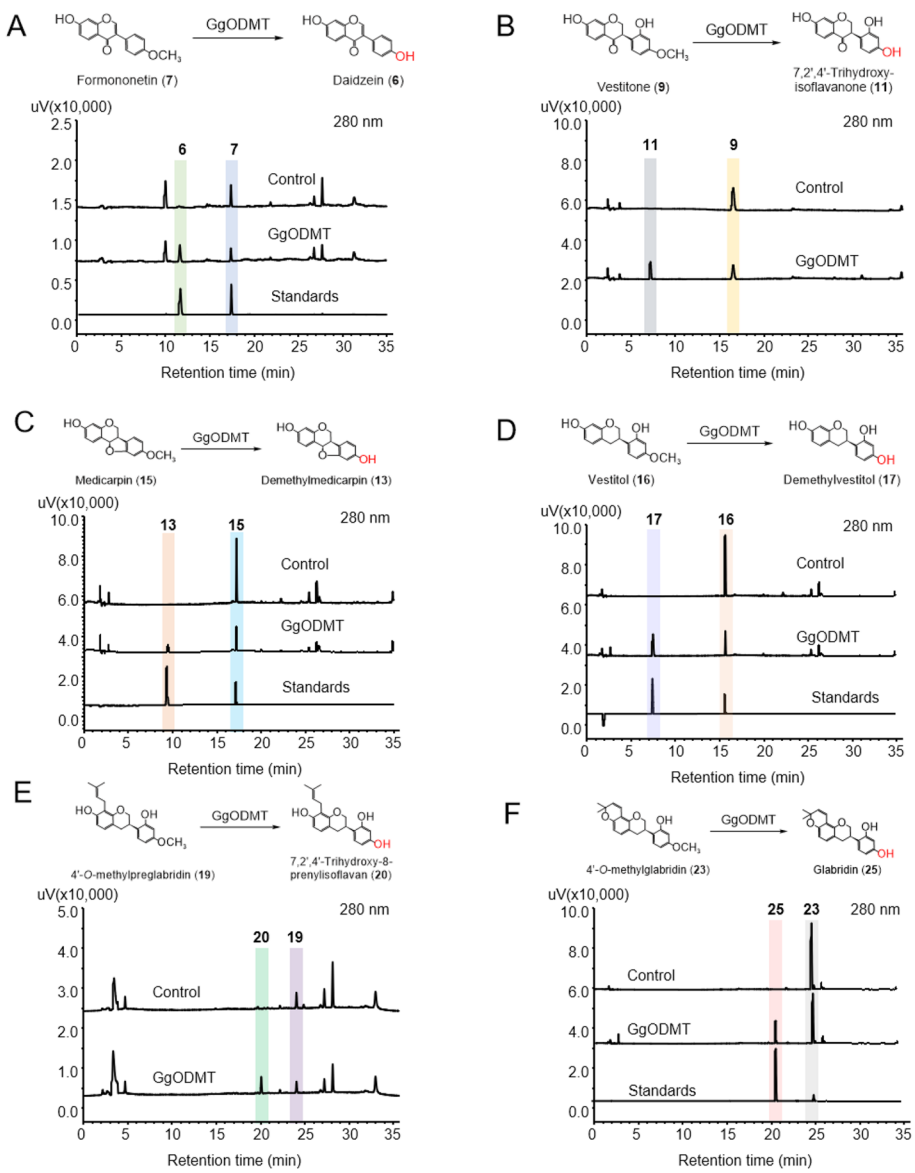


Fig. 4 ODMT participates in the biosynthesis of glabridin. **A**-**F** Functional characterization of GgODMT catalyzing various substrates in vitro. Shown are HPLC chromatograms of the enzymatic reactions

Shirazi et al. 2018), significant variation in transformation efficiency across different genetic backgrounds underscores the need for systematic optimization.

Hairy root induction efficiency is influenced by multiple factors, including *Agrobacterium* strain, explant type, pre-culture conditions, and acetosyringone (AS) supplementation. Among explant types tested, including cotyledons, hypocotyls, and cotyledon-hypocotyl junctions (Fig. S14A), cotyledon-hypocotyl junctions exhibited the highest hairy root induction efficiency (44.01%), outperforming cotyledons (15.62%) and hypocotyls (3.70%) (Fig. S14B-C). Distinct morphological patterns were also observed among the induced roots from different explants. Comparison of four *A. rhizogenes* strains (A4, K599, MSU440, and C58C1) revealed that K599 and MSU440 yielded moderateinduction rates (~20%), superior to A4 and C58C1, though still suboptimal overall (Fig. S14D). Pre-culture of explants significantly enhanced transformation outcomes, likely by reducing stress and improving cellular receptivity to *Agrobacterium*. Pre-culturing explants for 12–24 h prior to infection enhanced hairy root induction rates by 2- to 3-fold, with the highest efficiency (71.11%) achieved at 12 h (Fig. S14E). Acetosyringone (AS), a phenolic compound

that activates *vir* gene expression in *Agrobacterium*, is a critical co-factor for successful transformation (Vanhala et al. 1995). Two AS supplementation strategies were evaluated: (1) supplementing AS in bacterial resuspension buffers (BRB) and (2) inclusion during co-cultivation. Supplementing BRB with AS significantly improved induction rates (40.00 to 48.03%), nearly doubling rates compared to LB control (16.88%) (Fig. S14F). Further optimization identified 150 μM as the optimal concentration, achieving 82.22% induction (Fig. S14G). In contrast, AS supplementation in co-cultivation medium (1/2 MS) offered limited benefits (58.33% at 50 μM) and proving cost-ineffective (Fig. S14H). Post-transformation bacterial suppression is essential for root development and contamination control. Cefotaxime (Cef), a commonly used antibiotic for *Agrobacterium* inhibition, was tested at concentrations ranging from 50–200 mg/L. While all concentrations effectively suppressed bacterial growth, 100 mg/L Cef yielded the highest hairy root induction rate (77.67%) (Fig. S14I). Collectively, these optimizations, particularly selection of the cotyledon-hypocotyl junction explant, 12-hour pre-culture, K599 strain, 150 μM AS in BRB, and 100 mg/L Cef, substantially improved transformation efficiency, providing a robust and scalable platform for downstream metabolic engineering and functional genomics in *G. glabra*.

Enhanced production of glabridin by overexpressing biosynthetic genes in hairy roots

To elucidate the biological roles of key biosynthetic genes, *GgIFR*, *GgTHIS*, *GgPTS*, *GgPTR*, and *GgODMT* and evaluate the utility of hairy roots as a production platform, we engineered *G. glabra* hairy root lines overexpressing N-terminally GFP-tagged versions of these genes. Based on their superior catalytic efficiency, GgTHIS1 and GgPTR1 were selected alongside GgIFR, GgPTS, and GgODMT for metabolic enhancement. At two months post-transformation, transgenic lines were screened using a LUYOR-3415 portable fluorescent detector (Fig. S15A-E). qRT-PCR analysis confirmed robust overexpression of respective target genes in each transgenic line compared to empty vector (EV) control (Fig. 5A-F).

Glabridin levels were quantified using methanol-assisted ultrasonic extraction followed by HPLC analysis. EV control lines, derived from wild-type S-12, produced an average of 0.011 mg/g DW glabridin. In contrast, *GgIFR*-overexpressing (*GgIFR*-OE) lines exhibited a 44-fold increase in glabridin accumulation (0.507 mg/g DW), reaching levels comparable to those of 4-year-old *G. glabra* main roots (0.466 mg/g DW). Among other transgenic lines, glabridin yields followed the hierarchy: *GgPTR1*-OE (0.287 mg/g DW) > *GgTHIS1*-OE (0.135 mg/g DW) > *GgODMT*-OE (0.0903 mg/g DW) > *GgPTS*-OE (0.071 mg/g DW) (Fig. 5F, Fig. S15G). These results demonstrate that targeted overexpression of biosynthetic enzymes in hairy roots can significantly boost glabridin production, with GgIFR as a major rate-limiting factor. The findings establish hairy roots as a scalable and efficient platform for the metabolic engineering and sustainable production of high-value phytochemicals.

Discussion

The overarching goal of this study was to decipher the biosynthetic architecture of glabridin in *G. glabra* and establish a scalable platform for its sustainable production through metabolic engineering. This effort was driven by the hypothesis that glabridin accumulation in licorice is governed by distinct, modular biosynthetic routes involving multiple enzymatic steps, and that targeting key biosynthetic nodes could substantially enhance its metabolite yield. Despite its immense commercial value, particularly in the cosmetic and pharmaceutical sectors, glabridin's low limited natural abundance and lack of a defined biosynthetic framework have impeded both mechanistic understanding and industrial scalability.

Our results demonstrate that glabridin accumulates predominantly in the roots of *G. glabra*, consistent with its ecological role in stress adaptation. Alkali stress and MeJA treatment significantly enhanced glabridin biosynthesis, reflecting the natural adaptation of licorice to arid, saline-alkali environments. The induction of glabridin by 5-azaC and hydroxylamine further suggests potential involvement of epigenetic and redox regulatory mechanisms, opening new avenues for stress-mediated metabolic engineering in medicinal plants.

We then employed a multi-pronged strategy integregating metabolomics, transcriptomics, in vitro enzyme assays, and synthetic biology. This approach led to the discovery of multiple stress and chemical inducers of glabridin accumulation, the elucidation of two interconnected biosynthetic routes, and the functional characterization of five core enzymes: GgIFR, GgTHIS1/2, GgPTS, GgPTR1/4, and GgODMT. These enzymes were further validated through heterologous expression, substrate conversion assays, and in vivo overexpression in engineered hairy root cultures.

A central conceptual advance of this study, is in the identification of two distinct glabridin biosynthetic routes: an OMT/ODMT-dependent pathway which involves methylation-demethylation cycles, and an OMT/ODMT-independent pathway that bypasses these modifications. Although glabridin lacks a 4′-*O*-methyl group, the presence of methylated intermediates in the OMT/ODMT-dependent route suggests that this

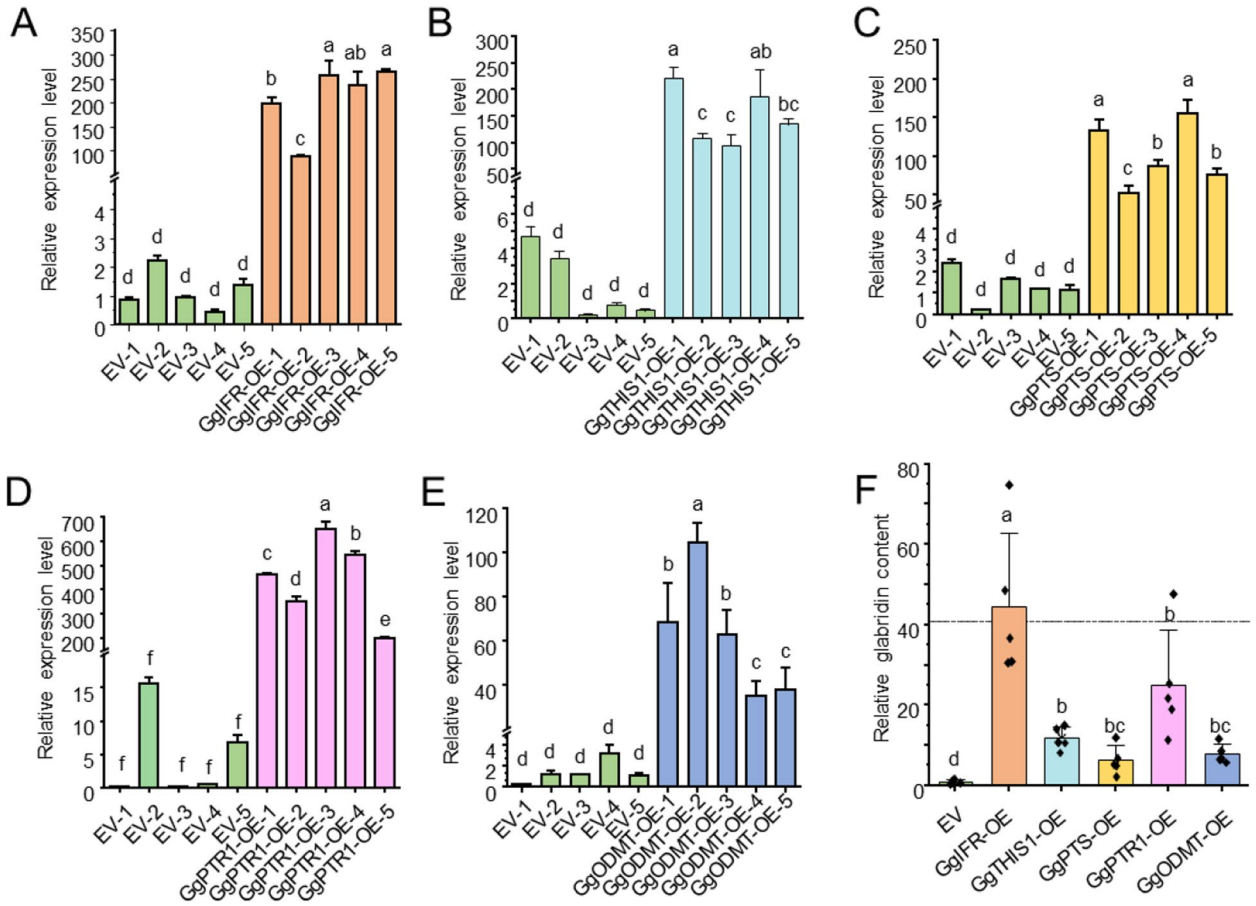


Fig. 5 Functional characterization of biosynthetic genes in vivo using *G. glabra* hairy roots. **A**-**E** qRT-PCR analysis of *GgIFR*-OE lines, *GgTHIS1*-OE, *GgPTS*-OE, *GgPTR1*-OE, and *GgODMT*-OE lines, respectively. **F** Relative glabridin contents in transgenic hairy roots. Data were normalized with test lines being calculated relative to the EV mean. The dashed reference line indicates the relative glabridin content in 4-year-old *G. glabra* main roots. Data are presented as mean ± SD; different lowercase letters denote statistically significant differences ($P < 0.05$)

seemingly inefficient cycle may serve regulatory or evolutionary roles. Indeed, similar intermediates and enzymes have been reported in other plant species, supporting the notion that this pathway is evolutionarily conserved. In contrast, the OMT/ODMT-independent route proceeds without the addition and subsequent removal of the *O*-methyl group. This study reveals that certain enzymes function exclusively within one pathway, whereas others participate in both (Fig. 3, Fig. S4, Fig. S11). Specifically, the broad substrate promiscuity of GgODMT in *O*-demethylation highlights its pivotal role in diversifying glabridin derivatives, potentially resolving the long-standing question of 4'-*O*-demethylation in glabridin biosynthesis. Notably, although GgODMT shares functional similarities with PsT6ODM and ObF7ODM1 as 2-ODD family demethylases, phylogenetic analysis reveals considerable evolutionary distance from them (Fig. S12A). With only ~50% sequence identity to these orthologs and lacking the distinctive N-terminal domain of ObF7ODM1, GgODMT may employ divergent catalytic mechanisms which requires validation through future structural studies and site-directed mutagenesis (Berim et al. 2015) (Fig. S16). The unavailability of numerous putative intermediates leaves open the possibility that GgODMT's substrate range extends beyond compounds tested, positioning it as a versatile biocatalytic tool for synthetic biology applications requiring diverse demethylation capabilities. This functional versatility contrasts with the strict regioselectivity observed in other 2-ODDs, highlighting how evolutionary divergence within enzyme families enables metabolic innovation in specialized plant pathways.

Different from the successful prenylation of **13** to **21** by PcM4DT, the unresolved catalysis of prenylation and cyclization steps remains a critical gap in glabridin biosynthesis. Despite testing seven PT and five CS candidates from *G. glabra*, no native enzyme activity was detected—like due to incomplete annotated genome or the presence of uncharacterized gene families. Horizontal

gene transfer or enzyme engineering may resolve this bottleneck. Collaborative approaches integrating deep genome mining, homology modeling, and in vitro reconstitution, akin to strategies used for glyceollin synthase characterization, are warranted to identify these missing components. More importantly, the efficient synthesis of glabridin through synthetic biology does not require that all genes need to be sourced from *G. glabra*. For example, ginsenosides are triterpene saponins accumulating specifically in *Panax* species, over 30 enzymes have been cloned and characterized to be involved in ginsenoside synthesis from *Panax* plants, yeast or bacteria (Yang et al 2018). However, all these genes need to be justified when used for industrial applications. Similarly, we have to be very cautious when using PcM4DT in synthesizing glabridin with synthetic biology approaches before its function is fully validated.

Complementing these discoveries, we optimized a high-efficiency *A. rhizogenes*-mediated hairy root transformation system tailored for *G. glabra*. By fine-tuning explant choice, bacterial strain selection, preculture duration, acetosyringone concentration, and post-infection antibiotic regimes, we achieved an induction efficiency exceeding 80%. This platform enabled precise in vivo validation of enzyme function and facilitated glabridin overproduction. Most significantly, transgenic hairy root lines overexpressing *GgIFR* exhibited a 44-fold increase in glabridin accumulation (0.507 mg/g DW), similar levels to those found in 4-year-old mature roots. Other engineered lines also showed significant improvements, with *GgPTR1*-OE and *GgTHIS1*-OE yielding 26-fold and 12-fold increases, respectively. These findings establish *G. glabra* hairy roots not only as a tractable model for functional genomics but also as a viable chassis for industrial-scale metabolite production.

To date, all reported efforts to synthesize glabridin or its intermediates have relied on yeast as the production chassis. In contrast, this study establishes *G. glabra* hairy roots as an potential and efficient platform. We show that using the *G. glabra* hairy root system to produce glabridin can potentially achieving high yields without the need to elucidate the entire biosynthetic pathway. By identifying treatment conditions that enhance glabridin accumulation in *G. glabra* plants, this study also demonstrates that this hairy roots system can leverage plant's endogenous regulatory mechanisms to toost glabridin production.

Taken together, this work provides the first comprehensive reconstruction of the glabridin biosynthetic network and identifies key enzymatic control points amenable to metabolic intervention. The dual-pathway model proposed here resolves longstanding questions regarding methylation dynamics and pterocarpan derivatization. Moreover, the successful deployment of a hairy root-based synthetic biology platform opens avenues for cost-effective, environment-independent glabridin production. These advances have immediate implications for the commercial biosynthesis of glabridin and broader applications in engineering legume-derived bioactives.

Materials and methods

Plant materials and growth conditions

Tissues of 4-year-old *G. glabra* and seeds used in this study harvested from Pingjibao germplasm garden in Ningxia. Seeds were sown on 1/2 MS (half-strength Murashige and Skoog) plates with 0.5 g/L MES (2-(N-morpholino) ethanesulfonic acid), 1.5% (W/V) sucrose, pH 5.8 after surface sterilization and overnight germination and grown under a 16-h-light/8-h-dark photoperiod at 25℃.

Seven-day-old seedlings were subjected to treatments containing drought, salt alkali, salt, high temperature, oxidative stress, and UVB, MeJA, ABA, methyltransferase inhibitors, histone acetyltransferase inhibitors and hydroxylamine inhibitors. Detail treatment parameters are shown in Table S1.

Compound extraction

To extract compounds from tissues or hairy roots for HPLC analysis, about 10 mg of freeze-dried samples were subjected to ultrasonic assisted extraction twice with 1 mL of methanol for 30 min each time, as described by Ma et al. (2024).

Transcriptional analysis

Seven-day-old seedlings were treated with 100 μM MeJA for 0, 1, 3 days, and with or without 10 mM $NaHCO_3$ for 12, 48 h. After treatment, seedlings were collected for transcriptomic analysis. Three biological replicates of each treatment were prepared. RNA extraction, library construction, sequencing, and analysis were performed by Gene Denovo Biotechnology Co., Ltd (Guangzhou, China). Total RNA was extracted using the Trizol method. RNA quality was assessed by agarose gel electrophoresis, NanoDrop, and Agilent 2100. Libraries were constructed using the NEB#7530 kit, and sequencing was performed on the Illumina HiseqTM 4000 platform. Differential expression analysis was conducted using the DESeq2 Bioconductor package. Genes with $|\log_2(\text{fold change})| \geq 1$ and adjusted p-value <0.05 were defined as differentially expressed genes (DEGs). Relevant result figures were

generated using the Gene Denovo Cloud platform or the TBtools software.

RNA extraction, cDNA synthesis and qRT-PCR were performed according to method used in Ma et al. (2024). The reference gene *actin* was used for normalizing the expression level (Maroufi 2016). The primers used are shown in Table S4.

Generation of constructs

For expression vectors in *E. coli* BL21(DE3), the CDS of candidate IFRs, THISs/VRs, PTS, PTRs, ODMTs were inserted into the pColdII vectors or pCold-TF vectors. For expression vectors in *S. cerevisiae*, the CDS of candidate PTs and CSs were inserted into the pESC-HIS vectors. For overexpression vector in hairy roots of *G. glabra*, the CDS were inserted into the pSuper1300 vectors to fuse with 5' end of *GFP*. The primers used in this study were listed in Table S4.

Expression and purification of recombinant proteins in *E. coli*

The heterologous expression and purification of recombinant proteins according to method described by Yang et al. (2024). The purified protein was stored at −80°C for further study.

Yeast microsome preparation

The yeast expression vectors were individually transformed into *S. cerevisiae* NMY51 or WAT11 strain, and the transformants were selected on SD/-His plates. The positive transformants were cultured overnight in liquid SD/-His media to reach their log growth phase, followed by centrifugation to collect the yeast cells. The collected cells were then washed twice with sterile dH_2O and incubated in SC/-His media with 2% (M/V) galactose for 24 h to induce the expression of target proteins.

Microsomes were prepared following the method described by Yang et al. (2020) with some modifications. Firstly, yeast cells were collected by centrifugation and resuspended with 1:1 (M:V) lysis buffer (50 mM Tris-HCl, pH 8.0, 1 mM PMSF, 1 mM EDTA, 5% glycerol). Then, the cells were ground in a mortar cooled with liquid nitrogen and diluted with a 5-fold volume of lysis buffer. Next,the cells lysates were centrifuged to collect the supernatants, which were then subjected to further centrifugation at 160,000 *g* for 90 min to isolate the microsomes. After centrifugation, microsomes were resuspended in storage buffer (50 mM Tris-HCl, pH 8.0, 1 mM DTT, 20% glycerol), and the concentration were measured with Bradford Protein Assay Kit (Beyotime, P0006).

Enzyme activity assay

For IFR activity assay, the reaction mixture was made with a total volume 100 μL consisted of 20 μg purified enzyme, 40 μM substrates, 100 mM potassium phosphate buffer (pH 7.0), and 1 mM NADPH. The reaction was carried out for 1 h at 30°C. For THIS/VR activity assay, the reaction mixture was made with a total volume of 100 μL consisted of 20 μg purified enzyme, 20–50 μM crude substrates, 100 mM potassium phosphate buffer (pH 6.0), and 1 mM NADPH. The reaction was carried out for 1 h at 30°C. For PTS activity assay, the reaction mixture was made with a total volume of 100 μL consisted of 20 μg purified enzyme, 20–50 μM crude substrates, 100 mM potassium phosphate buffer (pH 7.0). The reaction was carried out for 1 h at 30°C. For PTR activity assay, the reaction mixture was made with a total volume of 100 μL consisted of 100 μg purified enzyme, 4–20 μM substrates, 100 mM potassium phosphate buffer (pH 7.5), 0.1 mg/mL sucrose, and 0.5 mM NADPH. The reaction was carried out for 30 min at 30°C. For PT activity assay, the reaction system was made with a total volume of 100 μL containing 30 μg recombination yeast microsomes, 50 mM Tris-HCl (pH 8.0), 4–20 μM substrates, 1 mM DMAPP, and 10 mM Mg^{2+}. The reaction mixture was incubated at 20 ℃ for 2–8 h and followed by ethyl acetate extraction. For CS activity assay, the reaction system was made with a total volume of 100 μL containing 30 μg recombination yeast microsomes, 50 mM potassium phosphate buffer (pH 7.5), 20–50 μM crude substrates, and 1 mM NADPH. The reaction mixture was incubated at 25 ℃ for 6–8 h and followed by ethyl acetate extraction. For 2-ODD activity assay, the reaction mixture was made with a total volume of 100 μL consisted of 20 μg purified enzyme, 5–100 μM substrates, 100 mM potassium phosphate buffer (pH 6.0), 1 mM α-ketoglutarate and 1 mM ferrous sulfate. The reaction was carried out for 90 min at 25°C. The extracted solution was dried using a vacuum concentrator (Eppendorf, ag5305), dissolved in HPLC grade methanol, and filtered through 0.22 μm microporous membrane for further analysis. To obtain products for NMR identification, an enlarged reaction system was prepared to catalyze about 2 mg of substrates.

Generation of hairy roots

The recombinant vectors were introduced into *A. rhizogenes* strains (A4, K599, MSU440 or C58C1) via electroporation. Positive transformants were selected and cultured overnight at 30 °C agitation at with 200 rpm. The cultures were subsequently diluted 1:100 in fresh LB medium with proper antibiotics and grown until OD_{600} reached 0.6. Cells were collected by centrifugation and resuspended in different induction buffers to an OD_{600}

of 0.6. The suspension was incubated at 30 °C in darkness for 2 h before infection.

For infection, hypocotyls and/or cotyledons of 7-day-old *G. glabra* seedlings were immersed in the suspension for 30 min with gentle agitation. Following infection, the explants were blotted dry on sterile filter paper and transferred to co-cultivation medium (1/2 MS) for 48 h in darkness at 25 °C and then to selection medium consisting of 1/2 MS with cefotaxime sodium salt and cultured at 25 °C under 16/8 h (light/dark) photoperiod. Hairy roots will be observed after about 15 days.

HPLC and UPLC-MS analyses

The reaction products and compounds extracted from hairy roots were analyzed with HPLC. An HPLC system (SHIMADZU, LC-2030C) containing two reversed-phase C18 columns (150 mm × 4.6 mm, 5 μm, SHIMADZU; 250 mm × 4.6 mm, 5 μm, SHIMADZU) were employed. Gradient elution was performed using three mobile phases: A (water containing 0.1% formic acid), B (methanol) and C (acetonitrile). The gradient elution conditions were referred to one of the following two: (1) A and C were used: 0–7 min, 30% −33% A; 7–9 min, 33% A; 9–13 min, 33%−55% A; 13–15 min, 55% A, 15–27 min, 55%−90% A, 27–29 min, 90% A, 29–31 min, 90-30% A, 31–35 min, 30% A. (2) A and B were used: 0–25 min, 65%~50% A; 25–26 min, 50%−65% A; 26–30 min, 65% A.

To identify the products, a Thermo Scientific TSQ Endura LC-ESI-MS system with a UPLC Hypersil Gold column (100 x 2.1 mm 1.9 μm, Thermo Scientific) at 40 °C with a flow rate of 0.2 mL/min was used. Gradient elution was performed using two mobile phases: A (water containing 0.1% formic acid) and B (acetonitrile). The gradient elution condition were referred to one of the following two: (1) A and B were used: 0–7 min, 30% −33% A; 7–9 min, 33% A; 9–13 min, 33%−55% A; 13–15 min, 55% A, 15–27 min, 55%−90% A, 27–29 min, 90% A, 29–31 min, 90-30% A, 31–35 min, 30% A. (2) A and B were used: 0–25 min, 65%~50% A; 25–26 min, 50%−65% A; 26–30 min, 65% A. The injection volume was 1 μL. The wavelengths of the UV detectors were 210 nm, 254 nm, and 280 nm. The mass spectrometer operation parameters were set as follows: ion source temperature 250 °C, sheath gas 35 arb, auxiliary gas 10 arb, ion transfer tube temperature 275 °C, ion spray voltage 2.5 kV for negative mode and 3.5 kV for positive mode, and a mass scan range (*m*/*z*) of 150–800.

Abbreviations

I4′-OMT	4′-*O*-methyltransferase
I2′H	2′-hydroxylase
IFR	isoflavone reductase
VR	vestitone reductase
PTS	pterocarpan synthase
MeJA	methyl jasmonate
ABA	abscisic acid
5-azaC	5-azacytidine
THIS	7,2′,4′-Trihydroxyisoflavanol synthase:
PTR	pterocarpan reductase
ODMT	*O*-demethyltransferase
PT	prenyltransferase
DW	dry weight
CS	cyclase
HPLC	high performance liquid chromatography
NADPH	Nicotinamide Adenine Dinucleotide Phosphate Hydrogen
RT	retention time
DMAPP	Dimethylallyl diphosphate
2-ODD	2-oxoglutarate-dependent dioxygenase
AS	acetosyringone
BRB	bacterial resuspension buffer
Cef	Cefotaxime
EV	empty vector

Supplementary Information

The online version contains supplementary material available at https://doi.org/10.1186/s43897-025-00202-x.

Supplementary Material 1: Figure S1. The glabridin contents of samples for RNA-seq. (A) and (B) The glabridin contents of roots from 7-day-old seedlings with/without 10 mM $NaHCO_3$ or 100 μM MeJA were measured with HPLC. Glabridin contents were calculated based on dry weight. Data shown are from three biological repeats. (C) and (D) The correlation of RNA-seq samples and the number of differentially expressed genes (DEGs). Figure S2. Identification of IFR in *G. glabra*. (A) Protein sequence alignment of GmIFR (NP_001276127.2) and GgIFR. (B) Heatmap of GgIFR expression in transcriptomes under MeJA or $NaHCO_3$ treatments; numbers represent FPKM values. (C) MS and MS/MS spectra ($[M + H]^+$) of generated product **11**. Figure S3. Identification of VR and THIS in *G. glabra*. (A) Phylogenetic tree of GgVR/GgTHIS with MsVR (AAB41550.1), GmTHIS1 (Glyma.18G220500), and GmTHIS2 (Glyma.09G269600). (B) Expression heatmap of GgVR/GgTHIS in transcriptomes under MeJA or $NaHCO_3$ treatments; numbers indicate FPKM values. Figure S4. Functional characterization of GgVRs/GgTHISs in vitro. (A) Reaction scheme of THIS catalyzed transformation of **11** to **12**. (B) MS and MS/MS spectra ($[M - H_2O + H]^+$) of product **12**. (C) and (D) HPLC chromatogram and conversion rates of **11** to **12**. (E) Reaction scheme of VR or THIS catalyzed transformation of **9** to **14**. (F) MS and MS/MS spectra ($[M - H_2O + H]^+$) of product **14**. (G) and (H) HPLC chromatogram and conversion rates of **9** to **14**. Figure S5. Identification of PTS in *G. glabra*. (A) Nucleotide sequence alignment of *GgPTS* and *GePTS* (A0A1V1FH01). (B) and (C) MS and MS/MS spectra ($[M + H]^+$) of generated product **13** and synthetic standard **13**. Figure S6. Identification of PTR, PT and CYP71 in *G. glabra*. (A), (C) and (E) Phylogenetic tree of GgPTR, GgPT and GgCYP71. LjPTR1 (AB265589), LjPTR2 (AB265590), LjPTR3 (AB265591), LjPTR4 (AB265592), PcM4DT (AYV64464), GmG4DT (BAH22520), Glyma.11G062500 and Glyma.11G062600 were clustered. (B), (D) and (F) Expression heatmap of *GgPTR*, *GgPT* and *GgCYP71* in transcriptomes under MeJA and $NaHCO_3$ treatments; numbers indicate FPKM values. Figure S7. Characterization of the PT → PTR → CS pathway of glabridin biosynthesis. (A) and (B) Reaction scheme and HPLC chromatogram of PT catalyzed conversion of **13** to **21**. (C) MS and MS/MS spectra ($[M + H]^+$) of generated product **21**. (D) Reaction scheme of PTR catalyzed conversion of **21** to **20**. (E) MS and MS/MS spectra ($[M + H]^+$) of generated product **20**. (F) and (G) HPLC chromatogram and conversion rate of **21** to **20**. Figure S8 ^1H NMR and ^{13}C NMR of 3,9-Dihydroxy-4-prenylpterocarpan (**21**). (A) Structure of **21**. (B) ^1H NMR (500 MHz, Methanol-d4): δ 7.15 (1H, d, *J* = 8.3 Hz, *H*−1), 7.10 (1H, d, *J* = 8.0 Hz, *H*−7), 6.52 (1H, d, *J* = 8.4 Hz, *H*−2), 6.34 (1H, dd, *J* = 8.0, 2.2 Hz, *H*−8), 6.26 (1H, d, *J* = 2.2 Hz, *H*−10), 5.46 (1H, d, *J* = 5.6 Hz, *H*−11a), 3.50 (1H, m, *H*−6a) 3.47 (1H, m, *H*−6b). 5.19 (1H, t, *J* = 7.4 Hz, *H*−2′), 4.27 (2H, d, *J* = 5.9 Hz, *H*−1′), 1.76 (3H, s, *H*−4′), 1.65 (3H, s, *H*−5′). (C) ^{13}C NMR (126 MHz, MeOD): δ 161.95, 159.81, 156.94, 155.70, 131.46, 129.81, 126.01, 124.23, 119.74, 109.99, 108.58, 98.69, 80.70, 67.89, 49.51, 49.34, 49.17, 49.00, 48.83, 48.66, 48.49, 40.90, 25.93, 23.14, 17.87. Figure S9. Characterization of the PTR → PT → CS pathway of glabridin biosynthesis. (A) Reaction scheme of PTR catalyzed conversion of **13** to

17. (B) MS and MS/MS spectra ($[M + H]^+$) of generated product **17**. (C) and (D) HPLC chromatogram and conversion rate of **13** to **17**, respectively. (E) and (F) Reaction scheme and HPLC chromatogram of PcM4DT and candidate GgPT catalyzed conversion of **17**, respectively. (G) and (H) Reaction scheme and HPLC chromatogram of GmCS and candidate GgCS catalyzed conversion of **20**, respectively. Figure S10. Characterization of the PT → CS → PTR pathway of glabridin biosynthesis. (A) and (B) Reaction scheme and HPLC chromatogram of GmCS and candidate GgCS catalyzed conversion of **21**, respectively. (C) and (D) Reaction scheme and HPLC chromatogram of GgPTR catalyzed conversion of **24**, respectively. Figure S11. Functional characterization of GgPTRs. (A) and (B) Reaction scheme and HPLC chromatogram of GgPTRs catalyzed conversion of **13**, respectively. (C) and (D) Reaction scheme and HPLC chromatogram of GgPTRs catalyzed conversion of **15**, respectively. Figure S12. Identification of ODMT in *G. glabra*. (A) Phylogenetic tree of Gg2-ODDs with ObF7ODM1 (KM507365) and PsT6ODM (GQ500139). (B) Expression heatmap of *Gg2-ODDs* in transcriptomes under MeJA and $NaHCO_3$ treatments; numbers indicate FPKM values. (C) - (H) MS and MS/MS spectra ($[M + H]^+$) of GgODMT generated product. Figure S13. Enzyme properties of GgODMT. Effects of enzymatic reaction time (A), pH-dependence (B), temperature (C) on GgODMT activity. Figure S14. Induction of *G. glabra* hairy roots. (A) Seven-day-old aseptic seedlings of *G. glabra*. Scale bar = 2.0 cm. (B) One-month old hairy roots induced from different explants after infection. Scale bar = 2.0 cm. Effects of (C) infection positions, (D) *Agrobacterium* strains, (E) pre-culture duration, (F) Bacterial resuspension buffers (BRB), (G) and (H) AS concentration in infection solution and co-culture medium, respectively, and (I) cefotaxime (Cef) concentration in growth medium on hairy root induction rate. Data are presented as mean ± SD. Different lowercase letters indicate statistically significant differences ($P < 0.05$). Figure S15. Functional characterization of biosynthetic genes in vivo using *G. glabra* hairy roots. (A) - (F) Phenotypes of transgenic hairy roots: (A) *pSuper1300-GFP* empty vector (EV), (B) *GgIFR*-OE, (C) *GgTHIS1*-OE, (D) *GgPTS*-OE, (E) *GgPTR1*-OE, and (F) *GgODMT*-OE. Scale bars = 2.0 cm. (G) Glabridin contents in transgenic hairy roots. The dashed reference line indicates the glabridin level in main roots of 4-year-old *G. glabra*. Data are presented as mean ± SD. Different lowercase letters denote statistically significant differences ($P < 0.05$). Figure S16. Protein sequence alignment of PsT6ODM (GQ500139), ObF7ODM1 (KM507365) and GgODMT. Regions highlighted in red indicate the unique N-terminal domain of ObF7ODM1. Table S1. Summary of glabridin content variation of *G. glabra* under different treatment conditions. Table S2. Kinetic properties of GgODMT. Table S3. Comparison of GgVRs/THISs with reported VR/THIS protein sequences. Table S4. List of primers in this study.

Acknowledgements
The authors extend their gratitude to Drs. Haibo Tan and Zhongyu Zhou for providing valuable insights during the research process and manuscript preparation.

Authors' contributions
Yongqing Li, Ying Wang, Ling Yuan, Wei Sun and Hongxia Wang conceptualized the research. Ningxin Jiang, Xiaoling Ma, Yangxu Wu, and Xinyan Guo conducted the experiments. Yuping Li performed the bioinformatic analysis. Xiaoyi Wei proposed the two pathways. Ningxin Jiang, Xiaoling Ma, Xiaoyi Wei, Ling Yuan and Yongqing Li performed data analysis. Ningxin Jiang and Yongqing Li authored the manuscript. All authors have reviewed and approved the published version of the manuscript.

Funding
This research was funded by National Key Research and Development Program of China (2023YFC3504104), the Biological Resources Program, Chinese Academy of Sciences (KFJ-BRP-007-017), the Guangdong Provincial Key Laboratory of Applied Botany (2023B1212060046), the South China Botanical Garden, Chinese Academy of Sciences (Grant No: QNXM-02), the Shanghai Key Laboratory of Plant Functional Genomics and Resources, Shanghai Chenshan Botanical Garden (PFGR202502).

Data availability
All the underlying raw sequencing data of this article will be shared upon request to the corresponding author. The data supporting the findings of this work are available within the paper and its Supplementary Information files. The data sets generated and analyzed during this study are available from the corresponding author upon request. RNA-seq data generated during this study have been deposited at GSA database as a BioProject under accession PRJCA031681.

Declarations

Ethics approval and consent to participate
Not applicable.

Consent for publication
Not applicable.

Competing interests
The authors declare no conflict of interests.

Received: 5 June 2025 Accepted: 11 October 2025
Published online: 05 March 2026

References

Berim A, Kim MJ, Gang DR. Identification of a unique 2-oxoglutarate-dependent flavone 7-*O*-demethylase completes the elucidation of the lipophilic flavone network in basil. Plant Cell Physiol. 2015;56:126–36. https://doi.org/10.1093/pcp/pcu152.

Chiyo N, Seki H, Kanamoto T, Ueda H, Kojoma M, Muranaka T. Glycyrrhizin production in licorice hairy roots based on metabolic redirection of triterpenoid biosynthetic pathway by genome editing. Plant Cell Physiol. 2024;65:185–98. https://doi.org/10.1093/pcp/pcad161.

Gerszberg A, Wiktorek-Smagur A. Hairy root cultures as a multitask platform for green biotechnology. Plant Cell Tiss Organ Cult. 2022;150:493–509. https://doi.org/10.1007/s11240-022-02316-2.

Guo L, Paiva NL. Molecular cloning and expression of alfalfa (*Medicago sativa* L.) vestitone reductase, the penultimate enzyme in medicarpin biosynthesis. Arch Biochem Biophys. 1995;320:353–60. https://doi.org/10.1016/0003-9861(95)90019-5.

Hagel JM, Facchini PJ. Dioxygenases catalyze the *O*-demethylation steps of morphine biosynthesis in *opium poppy*. Nat Chem Biol. 2010;6:273–5. https://doi.org/10.1038/nchembio.317.

Hayashi H, Hiraoka N, Ikeshiro Y, Yamamoto H. Organ specific localization of flavonoids in *Glycyrrhiza glabra* L. Plant Sci. 1996;116:233–8. https://doi.org/10.1016/0168-9452(96)04387-7.

He JB, Dong ZY, Hu ZM, Kuang Y, Fan JR, Qiao X, et al. Regio-specific prenylation of pterocarpans by a membrane-bound prenyltransferase from *Psoralea corylifolia*. Org Biomol Chem. 2018;16:6760–6. https://doi.org/10.1039/c8ob01724g.

Hwang C, Yan S, Choe YM, Yun C, Xu SH, Im M, et al. Efficient hairy root induction system of *Astragalus membranaceus* and significant enhancement of astragalosides via overexpressing *AmUGT15*. Plant Cell Rep. 2024;43:285. https://doi.org/10.1007/s00299-024-03370-0.

Khatri P, Kuflu K, McDowell T, Lin J, Kovinich N, Dhaubhadel S. Discovery of three cytochrome P450 monooxygenase prenyl cyclases that catalyze the final step of glyceollin biosynthesis in soybean. Mol Plant. 2025;18(5):721–4. https://doi.org/10.1016/j.molp.2025.01.022.

Li YP, Xia CC, Luo M, Huang Y, Xia ZQ, Li YQ, et al. Comparative genomics of three medicinal *Glycyrrhiza* species unveiled novel candidates for the production of important bioactive compounds. Plant J. 2025;122:e70223. https://doi.org/10.1111/tpj.70223.

Li YP, Xie ZY, Huang Y, Zeng JY, Yang C, Yuan L, et al. Integrated metabolomic and transcriptomic analysis provides insights into the flavonoid formation in different *Glycyrrhiza* species. Ind Crops Prod. 2024;208:117796. https://doi.org/10.1016/j.indcrop.2023.117796.

Lu CJ, Du R, Fu H, Zhang JH, Zhao M, Wei YJ, et al. Heterologous biosynthesis of medicarpin using engineered *Saccharomyces cerevisiae*. Synth Syst Biotechnol. 2023;8:749–56. https://doi.org/10.1016/j.synbio.3.
Lu YF, Ding Z, Zhang DY, Zhu FY, Gao B. Integrated metabolomic and transcriptomic analysis reveals the pharmacological effects and differential mechanisms of isoflavone biosynthesis in four species of *Glycyrrhiza*. Int J Mol Sci. 2025;26:2539. https://doi.org/10.3390/ijms26062539.
Ma XL, Jiang NX, Fu JQ, Li YP, Zhou LJ, Yuan L, et al. A cytosine analogue 5-azacitidine improves the accumulation of licochalcone A in licorice *Glycyrrhiza inflata*. J Plant Physiol. 2024;292:154145. https://doi.org/10.1016/j.jplph.2023.154145.
Maroufi A. Selection of reference genes for real-time quantitative PCR analysis of gene expression in *Glycyrrhiza glabra* under drought stress. Biol Plant. 2016;60:645–54. https://doi.org/10.1007/s10535-016-0601-y.
Mirmazloum I, Slavov AK, Marchev AS. The untapped potential of hairy root cultures and their multiple applications. Int J Mol Sci. 2024;25:12682. https://doi.org/10.3390/ijms252312682.
Morey KJ, Peebles CAM. Hairy roots: an untapped potential for production of plant products. Front Plant Sci. 2022;13:937095. https://doi.org/10.3389/fpls.2022.937095.
Shirazi Z, Aalami A, Tohidfar M, Sohani MM. Metabolic engineering of glycyrrhizin pathway by over-expression of beta-amyrin 11-oxidase in transgenic roots of *Glycyrrhiza glabra*. Mol Biotechnol. 2018;60:412–9. https://doi.org/10.1007/s12033-018-0082-7.
Srivastava M, Singh G, Sharma S, Shukla S, Misra P. Elicitation enhanced the yield of glycyrrhizin and antioxidant activities in hairy root cultures of *Glycyrrhiza glabra* L. J Plant Growth Regul. 2019;38:373–84. https://doi.org/10.1007/s00344-018-9847-2.
Srivastava S, Srivastava AK. Hairy root culture for mass-production of high-value secondary metabolites. Crit Rev Biotechnol. 2007;27:29–43. https://doi.org/10.1080/07388550601173918.
Sun YL, Chen C, Lin C, Zhang H, Lian JZ, Hong BK. Elucidation and *de novo* reconstitution of glyceollin biosynthesis. Mol Plant. 2025;18:820–32. https://doi.org/10.1016/j.molp.2025.04.003.
Tenea GN, Calin A, Gavrila L, Cucu N. Manipulation of root biomass and biosynthetic potential of *Glycyrrhiza glabra* L. plants by *Agrobacterium rhizogenes* mediated transformation. Rom Biotechnol Lett. 2008;13:3922–32 (https://www.academia.edu/63630076).
Uchida K, Akashi T, Aoki T. The missing link in leguminous pterocarpan biosynthesis is a dirigent domain-containing protein with isoflavanol dehydratase activity. Plant Cell Physiol. 2017;58:398–408. https://doi.org/10.1093/pcp/pcw213.
Vanhala L, Hiltunen R, Oksman-Caldentey KM. Virulence of different *Agrobacterium* strains on hairy root formation of *Hyoscyamus muticus*. Plant Cell Rep. 1995;14:236–40. https://doi.org/10.1007/BF00233640.
Wahab S, Annadurai S, Abullais SS, Das G, Ahmad W, Ahmad MF, et al. *Glycyrrhiza glabra* (Licorice): a comprehensive review on its phytochemistry, biological activities, clinical evidence and toxicology. Plants. 2021;10:2751. https://doi.org/10.3390/plants10122751.
Wawrosch C, Zotchev SB. Production of bioactive plant secondary metabolites through in vitro technologies—status and outlook. Appl Microbiol Biotechnol. 2021;105:6649–68. https://doi.org/10.1007/s00253-021-11539-w.
Xie J, Tian J, Khan S, Chen F, Yu J, Hao Y, et al. Glyceollin biosynthesis in a plant chassis engineered for isoflavone production. Nat Chem Biol. 2025. https://doi.org/10.1038/s41589-025-01914-3.
Yang JL, Hu ZF, Zhang TT, Gu AD, Gong T, Zhu P. Progress on the studies of the key enzymes of ginsenoside biosynthesis. Molecules. 2018;23:589. https://doi.org/10.3390/molecules23030589.
Yang JL, Zhou T, Jiang Y, Yang B. Substrate specificity change of a flavonoid prenyltransferase AhPT1 induced by metal ion. Int J Biol Macromol. 2020;153:264–75. https://doi.org/10.1016/j.ijbiomac.2020.03.005.
Yang XM, Yang MZ, Ye P, Li HX, Li ZX, Zeng SH, et al. Characterization of dicaffeoylspermidine derivatives related glucosyltransferases during fruit development of goji berry. Food Chem. 2024;442:138432. https://doi.org/10.1016/j.foodchem.2024.138432.
Zeng JY, Ma XL, Li YP, Zhou LJ, Fu JQ, Wang H, et al. Histone deacetylases repress the accumulation of licochalcone A by inhibiting the expression of flavonoid biosynthetic pathway-related genes in licorice (*Glycyrrhiza inflata*). Mol Hortic. 2025;5:32. https://doi.org/10.1186/s43897-025-00144-4.

Publisher's Note

Springer Nature remains neutral with regard to jurisdictional claims in published maps and institutional affiliations.